NUCLEAR INSTRUMENTS AND METHODS 164 (1979) 267-278; © NORTH-HOLLAND PUBLISHING CO.

ACOUSTIC DETECTION OF HIGH ENERGY PARTICLE SHOWERS IN WATER

G. A. ASKARIYAN

P. N. Lebedev Physical Institute, USSR Academy of Sciences, Moscow, U.S.S.R.

B. A. DOLGOSHEIN, A. N. KALINOVSKY

Moscow Physical Engineering Institute, Moscow, U.S.S.R.

and

N. V. MOKHOV

Institute of High Energy Physics, Serpukhov, U.S.S.R.

Received 27 February 1979

The thermo-acoustic mechanism of sound generation by charged particles is analysed. The general procedure for calculating the fields of such acoustic radiation has been developed. The characteristics of an acoustic signal are calculated, which are in good agreement with the data of experiments[9]) on charged-particle beams. Calculations are made of ultrasonic radiation arising from the development of hadronic-electromagnetic cascades in water. Consideration is given to the potentialities of the acoustical method for detection of cosmic neutrinos in the ocean and for detection of particles in accelerator experiments.

1. Introduction

The idea of using the ocean as a detector of high-energy neutrinos[1]) has been wide-spread. The program of neutrino investigations and methods of neutrino detection at large depths in the ocean are now being intensively discussed[2-4]). Of great interest is a very promising acoustical method of charged particle detection[5-8])* in connection with its possible use in deep underwater neutrino experiments (the DUMAND project), as well as in massive (($\sim 10^4$ t) detectors for neutrino experiments to be performed at accelerators. The basic characteristics of acoustic radiation, calculated in ref. 6 from the thermo-acoustic mechanism of sound generation in liquid by charged particles, were confirmed experimentally[9]). Good agreement of experiment with theory[6]) provides a basis for a more elaborate development of theory and methods of calculation of an acoustic signal.

Calculations of the acoustic effects from ionizing radiation, which have been made quite recently[10,11]), do not represent, unfortunately, sufficiently rigorous solutions of a wide range of real problems. So they can claim only to provide a semi-quantitative description of processes while concrete results: an accurate spatial distribution of radiation, the shape, spectrum and amplitude of an acoustic signal, i.e., a comprehensive quantitative description of the field of acoustic radiation, cannot be obtained without simplifying assumptions and incorporation of free parameters.

In the present paper, which is a further development of the studies of refs. 6 and 12, we consider the thermo-acoustic mechanism of sound generation and the procedure for calculation of an acoustic signal on the basis of the known solutions by Kirchhoff and Poisson of wave equations (see, for example, ref. 13) and their spectral decompositions with allowance for sound absorption. The calculated characteristics of an acoustic signal are compared with the experimental data and calculation is made of the hadronic-electromagnetic cascade (HEC) and a resulting ultrasonic pulse.

2. The thermo-acoustic mechanism of sound generation and calculation of a sonic signal

Let us consider the process of transfer of the energy deposited on the tracks of charged particles in matter. It was shown in ref. 14 that the possible mechanisms of energy dissipation are characterized by a time that is much longer than the time of energy deposition on a track, i.e., energy on a track is deposited instantaneously. Among the possible energy dissipation mechanisms, the hydrodynamic mechanism is characterized by the shortest time $\tau_{HD} \sim l/c_s$ (l is the transverse track size and c_s is the velocity of sound, $c_s = 1.5 \times 10^5$ cm/s for water).

* It should be noted that in ref. 7 the acoustic signal values were overestimated by a factor 10^7–10^8.

The temperature conductivity mechanism, for example, is characterized by the time $\tau_{TC} \simeq l^2/\varkappa$ ($\varkappa$ is the coefficient of temperature conductivity, $\varkappa = 1.4 \times 10^{-3}$ cm^2/s for water). Therefore, $\tau_{HD} < \tau_{TC}$ even at $l > 10^{-8}$ cm whereas the track size is $l \sim 10^{-6}$ cm [15]). On account of the short characteristic time the hydrodynamic mechanism turns out to be the most efficient mechanism of energy transfer to matter. Its applicability is determined by the fact that the characteristic linear dimensions of the perturbation region are greater than intermolecular distances[14]).

A hydrodynamic pulse on the particle track contains frequencies up to $f_{max} = c_s/l$ [at high ionization densities – alpha particles, nuclear fragments – even conditions for the production of shock waves arise[14])]. In this case the greatest fraction of energy falls within the region of maximum frequencies[6]) which are absorbed at distances of about 1 μm in the vicinity of the track. Thus, thin heated filaments serve as radiators of sound in the hadronic–electromagnetic cascades in matter, which are of principal interest as regards the acoustical methods of detection. Obviously, the "fine structure" of an acoustic antenna, which the HEC is in matter, is important only in radiation of sound oscillation with wavelength $\lambda \leq \delta$ (δ is the mean distance between heated filaments). As calculations[6]) suggest and as will be demonstrated below, detection of the HEC in water is feasible at energies $E_0 \gtrsim 10^{14}$ eV. At these energies the number of particles in a shower is sufficiently large so that $\delta \ll d$, where d is the effective transverse dimension of the HEC (e.g. $\delta \lesssim 2 \times 10^{-2}$ cm $\ll d \simeq 5$ cm for $E_0 \gtrsim 10^{14}$ eV). Here, on account of interference between the various points across the HEC the effective range of radiation frequencies $f_{eff} = c_s/2d = 15$ kHz [6]) (see also below). It is this frequency range that is interesting in practice from the standpoint of sound absorption in water (the length of sound absorption at these frequencies is of the order of one kilometer). It thus appears that the structure of heated filaments may affect only the high-frequency ($f \sim c_s/\delta$) part of the acoustic radiation detectable within the region of the HEC. As regards the region outside the HEC, the relatively low-frequency acoustic radiation, which is only slightly absorbed in liquid and detectable at large distances, may be considered to be due to the averaged space-continuous energy deposition from the HEC. The simplest mechanism of generation of this radiation – the thermo-acoustic one – consists in the production of a sonic wave as a result of rapid expansion of liquid in the energy deposition region. It should be noted that expansion of liquid depends upon the total energy deposition Q but not on its distribution over the region of the HEC: $\Delta V = \alpha V \Delta T = \alpha V Q/VC\rho = \alpha Q/C_p$, where α is the thermal expansion coefficient, C_p is the specific heat capacity of the medium and ρ is the density of the medium.

The equation describing propagation of sound in water due to the thermoacoustic mechanism appears as

$$\Delta P - \frac{1}{c_s^2}\frac{\partial^2 P}{\partial t^2} = -\frac{\alpha}{C_p}\frac{\partial^2 q(\boldsymbol{r}, t)}{\partial t^2}. \tag{1}$$

Here $P(r, t)$ is the acoustic pressure, $q(r, t)$ is the energy deposition density. The solution to this equation is given by the Kirchhoff integral

$$P(\boldsymbol{r}, t) = \frac{\alpha}{4\pi C_p}\int \frac{\mathrm{d}V'}{|\boldsymbol{r}-\boldsymbol{r}'|}\frac{\partial^2}{\partial t^2} q\left(\boldsymbol{r}', t - \frac{|\boldsymbol{r}-\boldsymbol{r}'|}{c_s}\right). \tag{2}$$

Now consider the generation of a sonic signal by irradiation of liquid with a beam of charged particles or from the development of the HEC initiated by a high energy particle. The development of the HEC in space occurs in a time $\tau_h \sim 10^{-8}$ s, which is much shorter than the sonic signal duration $\tau_s \sim 10^{-5}$ s. In the case of a particle beam usually $\tau_b \ll \tau_s$, where τ_b is the beam spill time and $\tau_s = d/c_s$, d being the beam diameter. It may thus be assumed that energy is deposited instantaneously:

$$\dot{q}(\boldsymbol{r}, t) = q(\boldsymbol{r})\,\delta(t). \tag{3}$$

Using this relation, we can significantly simplify expression (2) for the signal pressure by writing it as*

$$P(\boldsymbol{r}, t) = \frac{\alpha}{4\pi C_p} c_s^2 \frac{\partial}{\partial R}\int_{S_r^R} \mathrm{d}\sigma \frac{q(\boldsymbol{r})}{R}. \tag{4}$$

Here the integration is over the spherical surface of the radius $R = c_s t$ with its centre at a detection point $\boldsymbol{r}$.

Solution (4) (Poisson formula) does not involve the frequency dependence explicitly and so it does not permit one to take accurate account of sound absorption, which is a function of frequency, or the frequency characteristics of a transducer. Thus,

* It is interesting to note that this expression is basically the Poisson formula for solving a homogeneous wave equation with the initial conditions: $P(\boldsymbol{r}, 0) = (\alpha/C_p)q(\boldsymbol{r})$ and $\partial/\partial t\, P(r, 0) = 0$.

solution (4) holds when (a) sufficiently wide-band transducers are used and (b) distances to the HEC $R \ll L(f)$, where $L(f)$ is the length of sound absorption at frequency f. As has been stated above, the effective range of radiation frequencies is $\sim 10-20$ kHz. This leads to real limitations $R \lesssim 100$ m. The results obtained by the Poisson formula (neglecting absorption for the whole frequency range) were compared with those including sound absorption [see below, expression (8)] in the frequency range $\lesssim 50$ kHz at a point $R = 100$ m. The results obtained with both methods agree within 20–30% (see also figs. 17a and 17b).

When calculating a sonic signal at large distances from the source one should take account of sound absorption which is significantly dependent on frequency. Applying the Fourier transform to the left and right sides of expression (2 with allowance for relation (3)] and incorporating a function χ, which accounts for sound absorption, for the frequency component of the pressure we have

$$P_\omega = -i\omega \frac{\alpha}{4\pi C_p} \int dv' \frac{\chi(\omega)}{|r-r'|} e^{i\frac{\omega}{c_s}|r-r'|} q(r). \quad (5)$$

The numerical integration in the region of the HEC energy deposition involves technical difficulties due to the rapidly oscillating function $\sim \exp[i(\omega/c_s)|r-r'|]$ occurring in the integrand. The multiplicity of integral (5) can be reduced using the axial symmetry of the energy deposition distribution and the fact that the spatial distribution of energy in the HEC is approximated by the expression

$$q(Z, \rho) = \frac{1}{2\pi} \sum_{i=1}^{N} A_i(Z) \exp[-\rho/\lambda_i(Z)], \quad (6)$$

whereby

$$\int_0^{2\pi} d\varphi \int_0^\infty dZ \int_0^\infty \rho\, d\rho\, q(Z, \rho) = E_0.$$

In the case of large distances from the detection point ($R \gg \lambda_{eff}$, where λ_{eff} is the effective transverse dimension of the HEC energy deposition region) we may write

$$P_\omega = -i\omega \frac{\alpha}{4\pi C_p} \int \frac{\chi(\omega)}{R\sqrt{D}} \times \times \exp\left[i\frac{\omega}{c_s} R\sqrt{D}\left(1 - \frac{\rho}{RD}\cos\varphi\right)\right] \times \times q(Z, \rho)\, \rho\, d\rho\, d\varphi\, dZ,$$

where $D = 1 + (Z-z)^2/R^2$; Z, R are the coordinates of the detection point, and z, ρ are the coordinates of the point at which the energy deposition occurs: $dQ = q(z, \rho)\rho\, d\rho\, d\varphi\, dz$.

Using expression (6) as $q(z, \rho)$ and integrating over ρ and φ we get

$$P_\omega = -i\omega \frac{\alpha}{C_p} \frac{1}{4\pi R} \int_0^\infty dZ \frac{1}{\sqrt{D}} \times \times \sum_{i=1}^{N} \frac{A_i(Z)\, \lambda_i^2(Z)}{(1+\beta_i^2)^{\frac{1}{2}}} \chi(\omega)\, e^{i\frac{\omega}{c_s} R\sqrt{D}}, \quad (7)$$

where $\beta_i^2 = (\omega/c_s)^2\, \lambda_i^2/D$.

In order to determine the time dependence of the sonic signal we make use of the inverse Fourier transform

$$P(r, t) = \frac{\alpha}{C_p} \frac{1}{4\pi^2 R} \int_0^\infty \frac{dZ}{\sqrt{D}} \int_0^\infty \omega\, d\omega\, \chi(\omega) \times \times \sum_{i=1}^{N} \frac{A_i(Z)\, \lambda_i^2(Z)}{(1+\beta_i^2)^{\frac{1}{2}}} \sin\{\omega(T_0 - t)\}, \quad (8)$$

where $T_0 = R\sqrt{D}/c_s$.

The basis regularities involved in the formation of a field of acoustic radiation of the HEC can be obtained by representing the HEC energy deposition region as a thin cylindrical antenna. On the assumption that the HEC energy deposition is uniformly distributed in volume $V = \pi a^2 L$ (where a and L are the effective transverse and longitudinal dimension of the HEC, respectively), an expression was derived in ref. 6 for the frequency component of the sound pressure. In the near wave field ($L \ll R \ll L^2/\lambda = R^*$) at an optimum angle $L\cos\theta/\lambda \ll 1$ the frequency component of the sound pressure is given by

$$|P_\omega| = \frac{\omega}{4\pi^{3/2}} \frac{\alpha}{C_p} E/\sqrt{(RR^*)}, \quad (9)$$

where E is the HEC energy deposited within the volume V. In the far field ($R \gg R^*$)

$$|P_\omega| = \frac{\omega}{4\pi^2} \frac{\alpha}{C_p} \frac{E}{R} \frac{\sin X}{X}, \text{where } X = \lambda/2\pi < \cos\theta. \quad (10)$$

In the approximation of the cylindrical antenna the acoustic radiation has the following characteristic features:

1) The radiation is substantially coherent ($P_{eff} \sim \omega |p_\omega| \sim E$) in the frequency range $f \leq f_{cr} = c_s/2\pi\lambda$, where $2\pi\lambda \sim 2a$ is the diameter of the HEC energy deposition region. At $a = 2-3$ cm, $f_{cr} = 25$ kHz.

2) In the near field the radiation is quasi-cylindrical ($P_{\text{eff}} \sim 1/\sqrt{R}$) and exists in the region of a thin disc of diameter D of the order of the sound absorption length (~ 1 km at the frequency of ~ 25 kHz in sea water), the disc plane being perpendicular to the HEC axis.

3) The duration of a sonic pulse is $\tau \sim 2a/c_s \sim 10^{-5}$ s. As will be shown below, the basic characteristics of the acoustic radiation obtained with allowance for the real spatial energy deposition of the HEC are close to the corresponding characteristics of radiation of the cylindrical acoustic antenna.

3. Comparison of calculations with the results of experiments on particle beams

To verify the validity of the theory of ultrasonic radiation based on the thermoacoustic mechanism, the characteristics of a sonic signal were calculated under the conditions of proton beam experiments[9]). Calculations were made using the Poisson formula through numerical integration. The energy deposition region was simulated by a cylinder whose diameter and length were chosen to suit the experimental situation. At proton beam energies of 158 and 200 MeV the dependence of linear energy loss on the depth of particle penetration into the medium was taken into consideration. The thermal expansion coefficient was taken to be $\alpha = 2.3 \times 10^{-4}$/°C (water at 20 °C) and the heat capacity, $C_p = 4 \times 10^7$ erg/g · °C.

Fig. 1 shows the signal amplitude as a function of the energy deposition in water for absorption of a 200 MeV proton beam of 4.5 cm diameter (the path length being 30 cm). The signal was calculated at a point positioned 1 m off the beam axis and moving along the beam from $Z = 0$ (entrance of the beam) to $Z = 0$ cm (end of the range). The differences between curves 1 and 3 are due to a build-up in the proton energy loss at the end of the range (the Bragg peak, see fig. 2) and to the influence of the final dimensions of the energy deposition region on the signal value.

Fig. 2 presents the pressure signal amplitude as a function of the location of the detector along the Z axis parallel to the axis of the cylindrical region of the energy deposition of a 158 MeV proton beam, as well as the linear density of the energy deposition as a function of the beam penetration depth. The distance between the beam axis and the Z axis was $R = 8$ cm. One can observe good agreement with the experimental data[9]) given in the same figure. The spatial distribution of the sonic signal is

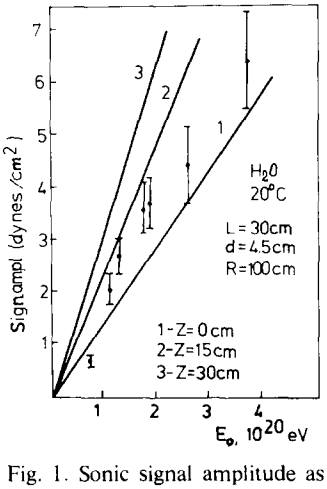

Fig. 1. Sonic signal amplitude as a function of the total energy depositon E_0. Circles denote the experimental data[9]).

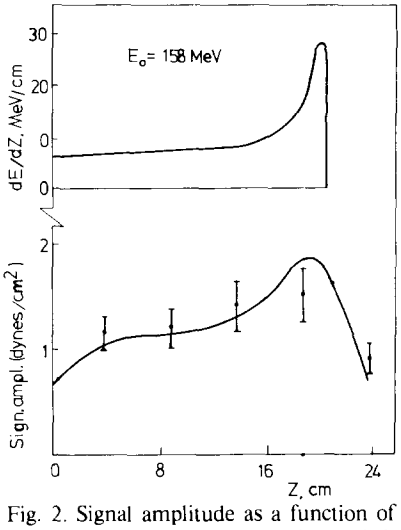

Fig. 2. Signal amplitude as a function of detector location (position). Circles denote the experimental data[9]).

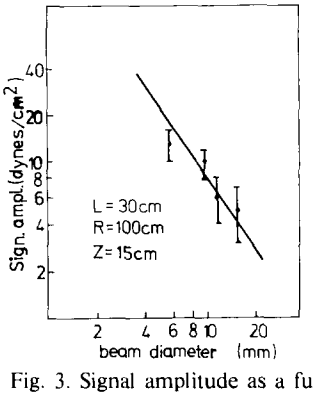

Fig. 3. Signal amplitude as a function of proton beam diameter. Circles denote the experimental data[9]).

significantly affected by nonuniformity of the linear energy loss (signal maximum in the region of the Bragg peak) and by the final dimensions of the energy deposition region (signal attenuation near the boundaries of the energy deposition region).

Fig. 3 displays the sonic signal amplitude as a function of the diameter of the energy deposition region (beam diameter).

The dependence of the sonic signal on the distance between the detector and the energy deposition region for various positions of the detector along the axis of a 200 MeV proton beam is shown in fig. 4.

A good agreement obtained between experiment and calculation based on the thermoacoustic mechanism of sonic radiation indicates that such mechanisms of sound generation as microbubbles, cavitation and other mechanisms do not seem to make significant contribution to the effect, in any case for water and for particles whose specific ionization is not substantially different from the minimum one. This statement is in disagreement with the experimental work of ref. 16 in which it has been concluded that the microbubble mechanism of sound generation is predominating.

The strongest argument in favour of the thermoacoustic mechanism of sonic radiation is the dependence of the sonic signal on the water temperature which is similar to that of the thermal expansion coefficient[9,17]*. Experiments[9]) revealed the fact that a sonic signal produced by charged particles in water becomes zero at $t = 5.7\,^{\circ}\mathrm{C}$ rather than at $t = 4\,^{\circ}\mathrm{C}$ ($\alpha = 0$). This fact cannot be explained by the microbubble mechanism of sound generation as in this case a sonic signal has to become zero at temperatures lower than 4 °C or does not have to become zero at all. Such a phenomenon may be attributed to electrostriction on the charged particle track, i.e., compression of the medium volume due to an electrostatic field arising from ionization. We shall estimate this effect.

* Such a dependence is also in disagreement with the results obtained in ref. 16.

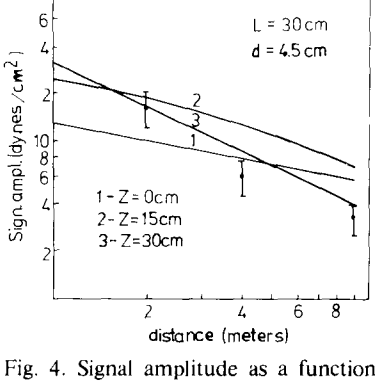

Fig. 4. Signal amplitude as a function of distance between the detector and beam axis. Circles denote the experimental data[9]).

A moving charged particle creates N_0 pairs of ions per unit length. This number of ion pairs decreases with the time because of recombination:

$$N(t) = N_0/(1+\beta n_i t),$$

where $n_i = 4\,N(t)/\pi l^2$ is the concentration of ions on the track with transverse dimension which equals $l[l = 0.5\times10^{-6}$ cm for water[15])]. The recombination coefficient $\beta = 1/n_i\tau$. Here τ is the time needed to bring two ions together:

$$\tau = \int_d^{d_{\min}} \mathrm{d}x/kE = \int_d^{d_{\min}} \frac{x^2\varepsilon}{kE}\,\mathrm{d}x = d^3\varepsilon/3\,ken_i,$$

where $d \simeq n^{-1}$ is the initial distance between two neighbouring ions, k is the ion mobility ($k \simeq 1$ CGSE), $E[x] = e/\varepsilon x^2$ is the electrostatic field of an ion and ε is the dielectric coefficient ($\varepsilon = 80$ for water). Then we obtain $\beta = ke/\varepsilon \simeq 2\times10^{-11}$.

At small distances from ions the interaction energy between ions and molecules becomes greater than the kinetic energy of a molecule, so a group of molecules is formed around each ion, i.e., local compression of the medium occurs. If the density of the medium is ρ, the concentration of molecules is n and their molecular weight is M, the volume of the medium per molecule is $V_1 = 1/n = M/\rho N_A$, where N_A is Avogadro's number. If a group consists of ν molecules, the change in volume of medium per ion will be $\Delta V_i = \nu(V_1 - V_0)$, where V_0 is molecular volume. Usually $V_1 \gg V_0$ and $\Delta V_i \simeq \nu V_1$.

In the conditions of the proton beam experiment[9]) [spill time is 50 μs, the proton energy is 158 MeV, the radius of the beam is 0.5 cm, the mean value of the number of ions is $\sim 5\times10^5$ (pair of ions)/cm] the changes in the volume of the medium due to the thermoacoustic mechanism and electrostriction will be, respectively

$$\Delta V_T \simeq \frac{\alpha}{C_p}\frac{j}{e}N_0 tW,$$

$$\Delta V_{ES} \simeq -\Delta V_i \frac{j}{e}N(t)\,Wt,$$

where j is the proton beam current, W is the energy needed for ion pair creation ($W = 30$ eV). Assuming the amplitude of sonic signal $P \sim (\Delta\ddot{V})$[6]), in an

effective frequency range $f_{\text{eff}} \simeq c_s/2a$ ($t_{\text{eff}} \simeq 2a/c_s$) we shall obtain

$$P_T \sim \frac{\alpha}{C\rho}\frac{j}{e} W \frac{N_0}{t_{\text{eff}}},$$

$$P_{ES} \sim -\frac{2\Delta V_{ES}}{t_{\text{eff}}^2}\frac{\pi l^2}{\beta}\frac{j}{e} = -\frac{2vM}{\rho N_0 t_{\text{eff}}^2}\frac{\pi l^2}{\beta}\frac{j}{e}.$$

The minus sign indicates the rarefaction signal.

Thus we obtain:

$$\left|\frac{P_{ES}}{P_T}\right| = \frac{vMC_p\pi l^2}{2\alpha W N_A t_{\text{eff}} N_0 \beta} \simeq \frac{10^{-5}}{\alpha} \quad \text{(assuming } v = 10\text{)}.$$

That is, the compression impulse amplitude becomes equal to the rarefaction one at $\alpha \simeq 10^{-5}$. That means that the sonic signal produced by the beam of charged particles in fresh water has to become zero at $t \simeq 6\,^\circ\text{C}$.

We note that the temperature curve of the sonic signal produced by absorption of a laser beam in water[17]), when electrostriction is absent, crosses the temperature axis exactly at $t = 4\,^\circ\text{C}$.

The electrostriction correction to the sonic signal produced by charged particles under the ordinary conditions is not significant ($\sim 10\%$ at $\alpha \simeq 10^{-4}$). This allows one to rely on the calculation procedure described above and based on the thermoacoustic mechanism of sound radiation for the prediction of pulsed acoustic fields arising from the development of hadronic-electromagnetic cascades in water.

4. Calculation of the HEC

When a high energy particle traverses a medium, a hadronic-electromagnetic cascade (HEC) arises. The appropriate field of the energy deposition, set up in a time $L/c \sim 10^{-8}$ s (where L is the effective cascade length and c is the velocity of light) determines an ultrasonic pulse. In the present paper we consider the HEC initiated in water by protons with energies from 400 to 10^7 GeV. It should be noted that the distribution of energy deposition in the HEC at high energies ($E_0 \gtrsim 10^3$ GeV) is practically independent of the kind of primary particle since at these energies the shape of the HEC is determined by the electromagnetic shower (EMS) initiated by gamma quanta of π^0-decay (see below). The calculation was made by Monte Carlo method with the use of the inclusive approach according to the MARS program[18]).

Calculations involved elastic and inelastic interactions between hadrons and hydrogen nuclei, inelastic interactions with oxygen nuclei, decays: $\pi^0 \to 2\gamma$, $\mu^{\pm} + \nu_\mu(\tilde{\nu}_\mu)$, energy loss of charged hadrons due to ionization and excitation of atoms, bremsstrahlung and pair production. To simulate hadron-nucleus interactions, use was made of phenomenological formulas[19]) describing the inclusive spectra of secondary hadrons. These formulas were verified up to energies of 2000 GeV by accelerator data and at higher energies by the data obtained in cosmic-ray experiments[20]).

In calculating the density distributions of the energy deposition, we took into account the contributions from the electromagnetic interactions of hadrons, the contributions of electromagnetic showers with allowance for their lateral and longitudinal development* and approximately the contributions from neutrons of energy $E < 10$ MeV, recoil nuclei and nuclear splitting. When calculating the EMS, we simulated the production of a π^0-meson, its decay into two gamma quanta and then simulated the gamma quantum range till the production of an electron pair. From this point the EMS was described by semiempirical formulas and the contribution of the energy deposition to the corresponding spatial cells was calculated.

The reliability of calculations in the range 20 MeV–400 GeV was verified by comparing them with numerous experimental data obtained at accelerators.

Since at high energies the main mechanism of

* In ref. 12 the contribution of the EMS to the total energy deposition was calculated in the approximation of its straightforward development, which overestimated the radial density gradient of the energy deposition near the axis of the HEC.

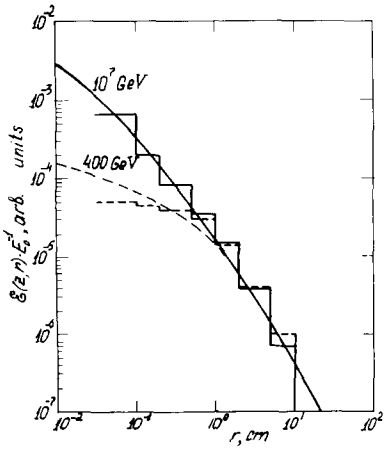

Fig. 5. Density of the energy depositon in the region of the maximum of the HEC initiated by protons and electrons (smooth curves: the calculation of ref. 21).

energy deposition is the EMS, the radial distributions of the energy deposition at the maximum of cascades initiated by a hadron and an electron must, in practice, be very similar. This is just confirmed by fig. 5 which shows, for two energies, the radial distributions of the energy deposited at the maximum of the cascade initiated by a proton (our calculation) and an electron (calculation of ref. 21).

Figs. 6–8 display some results of calculations of the HEC in water for primary energies of 400 and 10^7 GeV. The radial density distributions of the energy deposition have a shape representative of shower theory.

Figs. 7 and 8 illustrate the contributions of various energy deposition mechanisms to the radial and longitudinal distributions. One can observe the dominant role of the EMS at high energies.

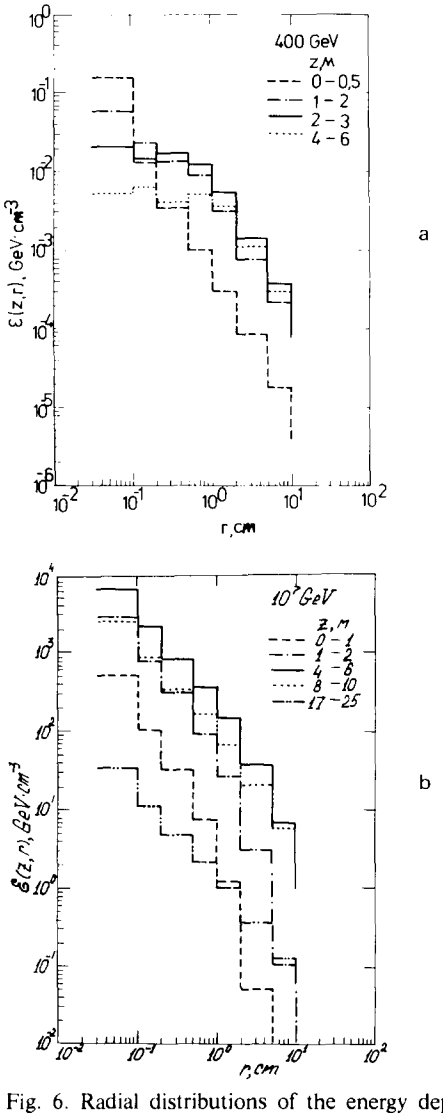

Fig. 6. Radial distributions of the energy deposition at various depths of the HEC development.

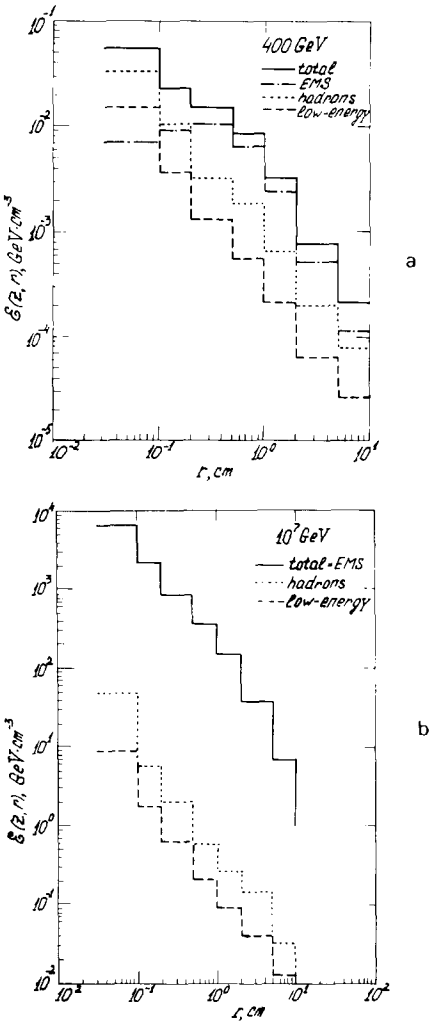

Fig. 7. Contribution of various mechanisms to the radial distributions of the energy deposition of the HEC.

The energy dependence of the basic characteristics of the HEC – position and value of the maximum separately for the energy deposition density and for the radius-integrated distributions – are presented in fig. 9. It can be seen that with increasing energy the maximum continuously shifts in the direction of primary particle motion and the energy deposition values at the maximum, divided by the primary energy, are practically independent of energy, starting from 10^4 GeV.

5. Calculation of a sonic signal from the HEC

In order to explore the potentialities of applying the acoustic method to detection of neutrinos in the

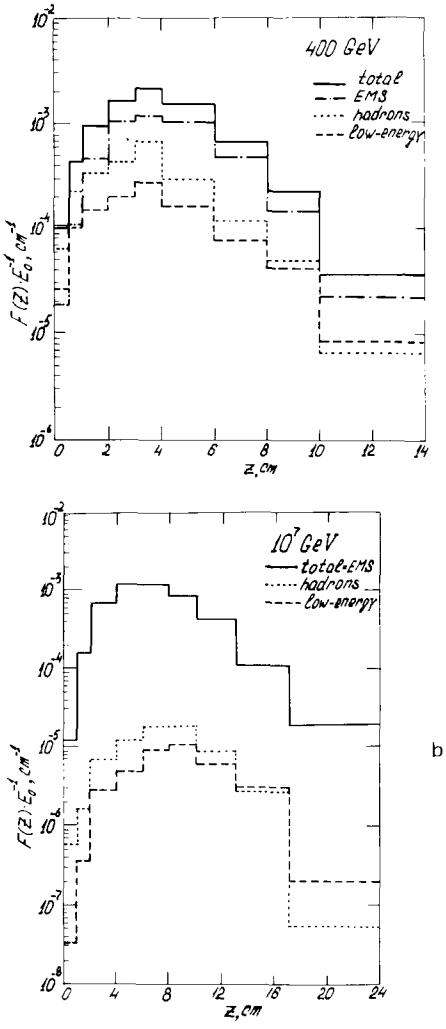

Fig. 8. Contribution of various mechanisms to the longitudinal distributions of the energy deposition of the HEC.

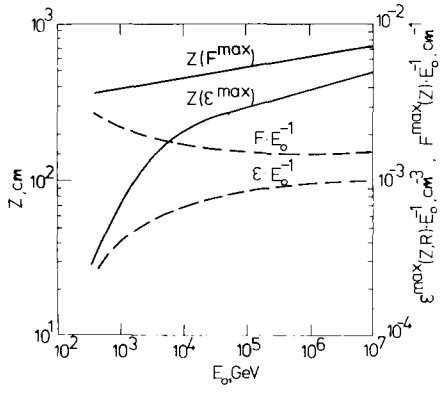

Fig. 9. Energy dependence of the position and value of the maximum separately for the radial and for the radius-integrated density of the energy deposition.

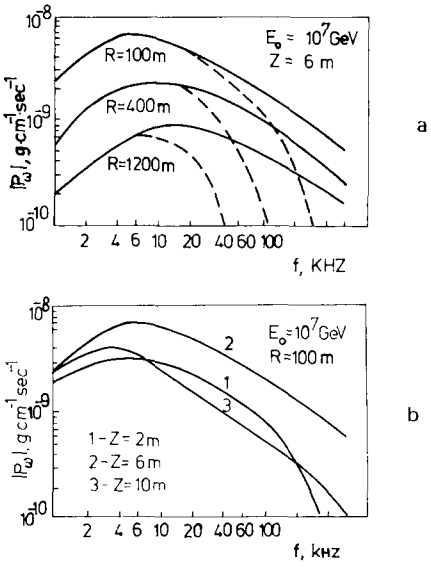

Fig. 10. (a) Frequency spectrum of the sonic signal for different distances between the detector and the HEC axis without (solid curves) and with sound absorption (broken curves). (b) Frequency spectrum of the signal for various positions of the detector along the HEC axis without sound absorption.

deep ocean and using this method in massive detectors at accelerators, we have calculated the characteristics of a sonic signal generated by the development of the HEC in water. The spatial density of the energy distribution in the HEC was approximated by expression (6) in which the first three terms were retained. In this case agreement with the distributions calculated by the Monte Carlo method was not worse than 30%. Special investigations have shown that the 30% uncertainty in the energy deposition density may lead, in the frequency range $f \leq 100$ kHz and at distances $R \geq 50$ m, to an uncertainty in the sonic signal value, which does not exceed 30% either. In the calculation of a sonic signal near the axis of the HEC ($R \lesssim 3r_{\text{eff}}$, where r_{eff} is the effective radius of the HEC) the uncertainty in the acoustic signal value increases.

As has already been indicated, when calculating a sonic signal at large distances from the sound source one should take account of sound absorption by the medium. The following expression was used as a function $\chi(\omega)$ including absorption of a sonic signal[22]):

$$\chi(\omega) = \exp(-0.115\eta S), \quad \eta = 0.036(\omega/2\pi)^{\frac{3}{2}}\ \text{dB/km},$$

where $S = |\boldsymbol{r} - \boldsymbol{r}'|$ is the distance from the detection point to the element of the volume $\mathrm{d}v'$ in which energy $q(\boldsymbol{r}')\mathrm{d}v'$ is deposited.

The thermal expansion coefficient for sea water at 5 km depth was taken to be $\alpha = 2.1 \times 10^{-4} °C^{-1}$ and the heat capacity of water, $C_p = 3.6 \times 10^7$ erg/g · °C [23])*.

Figs. 10a and 10b display the frequency spectra of the sonic signal from the HEC with an energy of 10^7 GeV for different locations of the detector. As is evident from the figures, the position of the maximum slightly shifts from a frequency of 20 kHz towards lower frequencies as the detector approaches the HEC. Softening of the sonic signal spectrum is also observed when the detector is moved along the axis of the HEC, which is due to broadening of the cascade at large depths of its development. It is also seen from fig. 10a that frequencies of $\gtrsim 50$ kHz contribute but little to the sonic signal*.

Fig. 11 presents the shape of the sonic signal in time for $f \lesssim 50$ kHz. The pressure signal represents two successive compression and rarefaction signals, each with an effective duration $\tau \sim 10-20$ μs. The position of the compression and rarefaction signals on the time scale $(t - R/c_s)$ and their duration indicate that the efficient source of sound in the HEC is a region near the axis with a radius of about 2 cm.

It is worth noting an interesting feature in the behaviour of the shape of the pressure signal with a change in the distance between the detector and the HEC. Namely, the ratio of the amplitude of the rarefaction signal to the compression signal, which is less than unity at small distances, increases with distance (see fig. 12). This phenomenon can be used to determine the distance from the detector to the HEC, which enables one, given the dependence of the sonic signal value on distance, to determine the HEC energy.

It is evident from figs. 10 and 11 that up to distances of 1000 m the sound absorption little affects the signal amplitude. Fig. 13 shows isobaric lines of equal amplitude of the signal pressure for the HEC with an energy of 10^7 GeV without allowance for sound absorption in water. The specific shape of isobaric lines, when information is extracted sufficiently comprehensively, may enable one to determine the direction of the HEC development[12]) and may also provide a more reliable

* As was pointed out in ref. 23, the value of α/C_p for sea water at 5 km depth coincides with the value of α/C_p for fresh water at $t = 20$ °C.

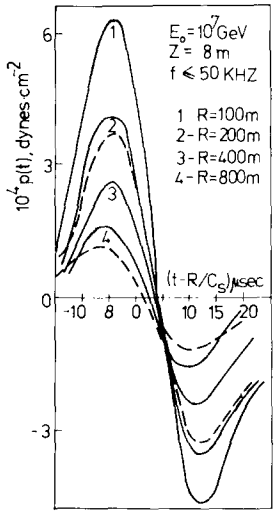

Fig. 11. Pressure signal shape with (broken curves) and without sound absorption (solid curves).

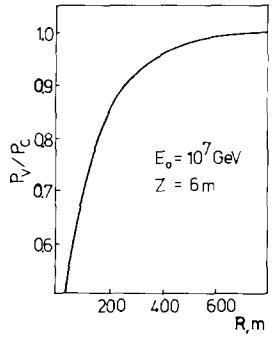

Fig. 12. Amplitude ratio of the rarefaction signal to the compression one as a function of distance between the detector and the HEC.

* Enrichment of the sonic signal spectrum with high frequencies in ref. 12 resulted from neglect of the radial spread of the EMS.

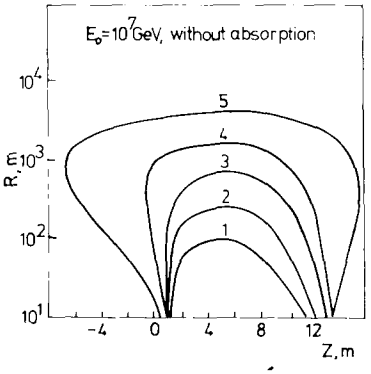

Fig. 13. Isobaric lines of the same signal amplitude. Curve 1 corresponds to a pressure of 6.2×10^{-4} dyn/cm^2, each subsequent curve corresponds to a pressure which is half as great as that of the preceding curve.

extraction of a useful signal against the background of random noise. The dependence of the signal amplitude on distance R in a transverse direction about the HEC axis for three values of Z is given in fig. 14.

The dependence of the signal on the HEC energy is shown in fig. 15. As the data presented suggest, this dependence is nearly linear ($\sim E^{1.07}$) in a wide range of HEC energies. A slight deviation from the linear increase of the signal may be explained by the fact that with increasing HEC energy the value of the energy deposition density gradient rises and so the contribution of high frequencies relatively increases.

Calculations were also made of the acoustic field for the HEC with an energy of 400 GeV, which are interesting when compared with experiments performed at FNAL [24]). The characteristics of sonic signals were calculated by Poisson formula (4), except for the results presented in fig. 17a which were calculated by formula (8). The applicability of the Poisson formula in the given case is due to the fact that the acoustic field is intended to be explored at distances of ~ 1 m from the axis of the HEC [24]) and sound absorption at such distances can be neglected. On the other hand, it is necessary to ensure a sufficiently wide-band reception (up to 100–200 kHz) when making measurements within the volume of the HEC, especially in the vicinity of its axis where the radial density gradient (see fig. 7a) may lead to a considerable contribution of high frequencies. The approximation of the continuous distribution of the energy deposition is also justified here since the amplitude of the signal in water from the HEC with an energy of 400 GeV ($\sim 10^{-7}$ dyn/cm^2, see below) is far beyond the possible range of detection ($\sim 10^{-3}$–10^{-4} dyn/cm^2). Therefore, detection is possible only for the case of simultaneous interaction of a group of protons with the total energy deposition $\gtrsim 10^{14}$ eV. This will lead to the fulfillment of the condition $\lambda_{min}(\sim 200\ \text{kHz}) \gtrsim \delta$, the mean distance between tracks (hot filaments).

Fig. 16 shows the dependence of the signal amplitude on the detector location. It is worth noting a drastic increase in the signal value as the axis of the HEC is approached. This may be explained by the fact that although the fraction of the energy deposited near the cascade axis is small compared with the total energy deposition, the efficiency of energy emission in the form of high-frequency sonic waves is high because of a large density gradient of the energy deposition. As a result of high sensitivity of the signal value on the cascade axis to the form of the radial distribution of the energy deposition near the axis, the signal amplitude value may comprise a factor 2 as an uncertainty.

The shape of the pressure signal is displayed in figs. 17a and 17b for different positions of the detector. The results presented suggest that the ratio of the amplitude of the rarefaction signal to the compression signal is 0.3–0.5, increasing with distance from the HEC. The results presented in

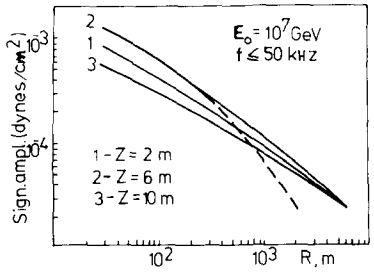

Fig. 14. Signal amplitude as a function of distance for various positions of the detector along the HEC axis. Solid curves, without sound absorption; broken curves, with sound absorption.

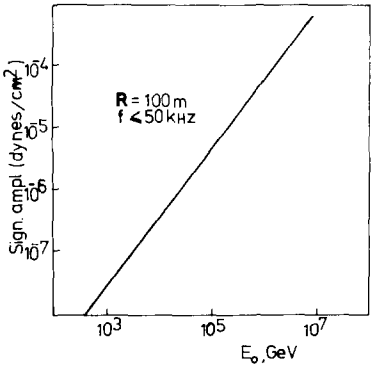

Fig. 15. Sonic signal amplitude as a function of energy of the HEC.

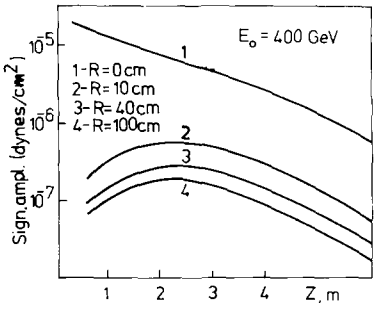

Fig. 16. Signal amplitude as a function of spatial arrangement of the detector for the HEC energy $E_0 = 400$ GeV.

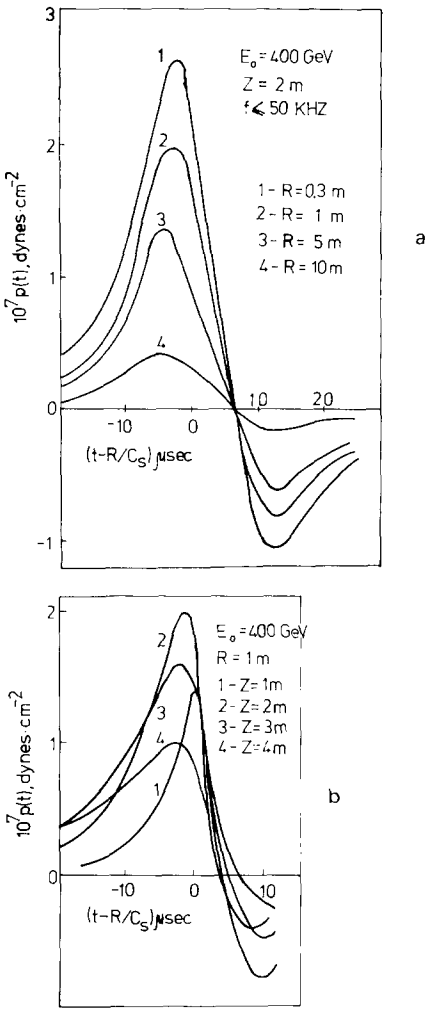

Fig. 17. (a) Pressure signal shape for different distances between the detector and the HEC with an energy of 400 GeV. (b) Pressure signal shape for various positions of the detector along the axis of the HEC with an energy of 400 GeV.

fig. 1b also imply that at distances comparable with the HEC length the shape of the pressure signal is very strongly dependent on the position of the detector along the cascade axis. More specifically, when the detector is moved in the direction of the HEC development there occurs a considerable increase in the duration of the pressure signal and the signal front becomes less steep (softening of the frequency spectrum of the signal) (see also fig. 10). This is due to a decrease in the density gradient of the energy deposition with increasing depth of the HEC development. From comparision of the shape of the pressure signal calculated by formula (8) (fig. 17a, curve 2) and by the Poisson formula (fig. 17b, curve 2) one can see that the use of a detector having a limited frequency band ($f \leq 50$ kHz) leads to a distortion of the signal shape (the duration increases and the signal front becomes less steep) as compared with the case when all frequencies are received.

6. Conclusion

The described procedure for calculation of sonic signals from particle showers in water enables one to obtain the total quantitative characteristics of the sonic field in the case of a random distribution of the energy deposited.

As has been demonstrated above, measurement of the characteristics of the acoustic field of the HEC in water (amplitude of the sonic signal, its spatial and time distributions, frequency characteristics, rarefaction-to-compression amplitude ratio, etc.) can give very useful information about the HEC: energy, direction of its development, width, spatial distribution of particles and the like. The realization of such a program is wholly dependent on the potentialities of detecting sonic signals which are very small in amplitude (see fig. 14).

It is expedient to consider two fields of possible application of the acoustic method of detection[6,9]). The first pertains to detection of cosmic neutrinos in the ocean [the DUMAND project[4])]. In this case, even if the noise level of hydrophones in the deep ocean were determined only by thermal noise[23]) ($P_{\text{therm}} = 10^{-4}$ dyn/cm^2·Hz$^{\frac{1}{2}}$ at a frequency of 20 kHz) neutrino-induced showers in water seem to be detectable only starting from energies of $\sim 10^{15}$ eV (a signal of $\sim 5 \times 10^{-5}$ dyn/cm^2 at a distance of 100 m, the signal-to-noise ratio ~ 1 when using a group of 10^3–10^4 hydrophones for detection of one cascade). The set-up of this type is intended to detect neutrinos of interstellar and intergalactic origin[4]) with energies $\gtrsim 10^{15}$ eV and is to have a volume of ~ 100 km^3 [4,6]).

The other possibility is associated with the manufacture of inexpensive, massive ($\sim 10^4$ t) detectors for accelerator physics[9]). As has been shown above, the signal from the cascade in water with an energy of 400 GeV will be as low as $\sim 10^{-7}$ dyn/cm^2 at a distance of ~ 1 m; so the use of acoustic detectors in water is feasible only starting from energies $\sim 10^{14}$ eV. Yet, detection of a single cascade of $\sim 10^{12}$ eV is feasible if one employs, instead of water, another liquid, having a much larger value of α/C_p, as a detecting medium. For example, $(\alpha/C_p)_{CCl_4}/(\alpha/C_p)_{H_2O} \simeq 50$ and the detectable sonic signal per unit energy deposited is also larger by a

factor of $\simeq 50$ [9]). We can mention the use of a large coherent array of detectors[25]) (signal-to-noise ratio $\sim\sqrt{N}$, where N is the number of detectors) as an additional possibility of reducing the energy threshold of detection.

All this gives good reasons to believe that the acoustical method of particle detection may find applications both at accelerators of the new generation and for detection of cosmic neutrinos in the ocean.

References

1) M. A. Markov, Proc. 10th Int. Conf. on *High energy physics*, Rochester (1960) p. 579; I. M. Zheleznykh and M. A. Markov, Physics of high energy neutrinos, D-577, Dubna (1960).
2) Proc. 1975 DUMAND Summer Workshop, Bellingham, Wash. (1976).
3) Proc. 1976 DUMAND Summer Workshop, Hawaii (1976).
4) V. S. Berezinsky and G. T. Zatsepin, Uspekhi Fiz. Nauk **5** (1977).
5) G. A. Askarian, Atomnaya Energiya **3** (1957) 152.
6) G. A. Askarian and B. A. Dolgoshein, Preprint no. 160, Lebedev Physical Institute of the USSR Academy of Sciences, Moscow (1976); G. A.Askarian and B. A. Dolgoshein, ZhETF pys'ma **25** (1977) 5; B. Dolgoshein, Proc. 1976 DUMAND Workshop, Hawaii (1976).
7) T. Bowen, Proc. 1976 DUMAND Workshop, Hawaii (1976).
8) L. Sulak, Proc. 1976 DUMAND Workshop, Hawaii (1976).
9) L. R. Sulak, Proc. Int. Conf. on *Neutrino physics and neutrino astrophysics*, vol. 2, Baksan Valley (1977); L. R. Sulak et al., Nucl. Instr. and Meth. **161** (1979) 203.
10) J. Learned, Proc. La Jolla Workshop on *Acoustic detection of neutrinos*, San Diego (1977); J. G. Learned, UCI Physics preprint, 7744 (1977).
11) T. Bowen, Proc. La Jolla Workshop on *Acoustic detection of neutrinos*, San Diego (1977).
12) G. A. Askarian, B. A. Dolgoshein, A. N. Kalinovsky and N. V. Mokhov, Preprint no. 140, Lebedev Physical Institute, Moscow (1977); G. A. Askarian, B. A. Dolgoshein, A. N. Kalinovsky and N. V. Mokhov, Proc. Int. Conf. on *Neutrino physics and neutrino astrophysics*, vol. 2, Baksan Valley (1977).
13) E. Skudrzyk, *Die Grundlagen der Akustik* (Wien, 1954).
14) V. I. Goldansky, E. Ya. Lantsburg and P. A. Yampolsky, ZhETF pys'ma **21** (1975) 6.
15) E. Kobetich and R. Katz, Phys. Rev. **170** (1968) 391.
16) V. D. Volovik, V. V. Petrenko and G. F. Popov, ZhTF pys'ma **3** (1977) 10.
17) P. I. Golubnichiy, G. S. Kalyuzhnyi and V. I. Yakovlev, Preprint 167, Lebedev Physical Institute, Moscow (1978).
18) N. V. Mokhov, Preprint 76-64, IHEP, Serpukhov (1976). I. S. Baishev, S. L. Kuchinin and N. V. Mokhov, Preprint 78-2, IHEP (1978).
19) L. R. Kimel and N. V. Mokhov, Izv. Vuzov (fizika) **10** (1974); N. V. Mokhov and Yu. P. Nikitin, in *Problems of nuclear and cosmic-ray physics*, vol. 6 (Kharkov, 1977).
20) E. A. Mamidzhanyan et al., Preprint 238 (31)-77, Erevan Physical Institute, Erevan (1977).
21) K. Kamata and J. Nishimura, Progr. Theor. Phys. Suppl. **6** (1958) 93.
22) G. N. Sverdlin, *Applied hydroacoustics* (Sudostroyeniye, Leningrad, 1976) (in Russian).
23) H. Bradner, Proc. La Jolla Workshop on *Acoustic detection of neutrinos*, San Diego (1977).
24) T. Bowen et al., Proposal for detector development study of acoustic calorimetry at Fermilab energies, FHAL (1977).
25) L. Sulak et al., Proc. La Jolla Workshop on *Acoustic detection of neutrinos*, San Diego (1977).